Dayside auroral hiss observed at South Pole Station

X. Yan,[1] J. LaBelle,[1] G. Haerendel,[2] M. Spasojevic,[3] N. Bunch,[3] D. I. Golden,[3]
H. U. Frey,[4] and A. T. Weatherwax[5]

Received 11 July 2012; revised 16 January 2013; accepted 17 January 2013.

[1] We performed a statistical study of low frequency (LF) auroral hiss recorded at South Pole Station in 2004, 2005, and 2007, and very low frequency (VLF) hiss recorded in 2000–2008. As expected, most auroral hiss occurs in the pre-midnight sector. However, there is a secondary peak in occurrence in the pre-noon sector (1000–1530 UT; ∼0630–1200 magnetic local time (MLT)) and somewhat more events occur in the post-noon sector (1530–2100 UT; ∼1200–1730 MLT), with a null in occurrence around noon MLT. Individual dayside events appear similar to nightside hiss, but statistically they do not extend to as high frequencies. Solar wind discontinuities or impulses on the magnetopause are not correlated with these events. All-sky camera, photometer, magnetometer, riometer, and VLF receiver data show that dayside LF hiss almost always extends to the VLF range and is often associated with active aurora. Examination of interplanetary magnetic field (IMF), substorm conditions, and Kp/AE/QI indices at times of dayside hiss suggests differences between the pre-noon and post-noon events: pre-noon events are associated with IMF $B_y < 0$, whereas post-noon events favor $B_z < 0$ and show a weaker correlation with $B_y > 0$. The correlation between pre-noon events and $B_y < 0$ may arise because under those conditions, the pattern of field-aligned currents (FACs) shifts to later magnetic local times, causing upward FACs to be dominant during pre-noon hours at 74°, the invariant latitude of the South Pole. Unlike pre-noon events, post-noon events are more often associated with substorm activity on the nightside and favor elevated Kp indices, suggesting a connection of post-noon events to nightside activity.

Citation: Yan, X., J. LaBelle, G. Haerendel, M. Spasojevic, N. Bunch, D. I. Golden, H. U. Frey, and A. T. Weatherwax (2013), Dayside auroral hiss observed at South Pole Station, *J. Geophys. Res. Space Phys.*, *118*, doi:10.1002/jgra.50141.

1. Introduction

[2] Auroral hiss was the first reported auroral radio emission [*Burton and Boardman*, 1933]. The names "hiss," coined by *Gallet* [1959], and "auroral hiss," coined by *Martin et al*. [1960], were derived from the sound made by the amplified broadband audio-frequency signals of the emissions. Early observations connected auroral hiss to the optical aurora [e.g., *Jørgensen and Ungstrup*, 1962]. Subsequent ground-level observations revealed two distinct types of auroral hiss: continuous hiss and impulsive hiss [see reviews by *Makita*, 1979; *Sazhin et al*., 1993; *LaBelle and Treumann*, 2002, and references therein]. Continuous hiss lasts for 1 h or longer, usually occurs at frequencies below 30 kHz, has relatively constant amplitude, and is structureless. Impulsive hiss typically lasts 1–5 min or less and has considerably greater bandwidth, extending above 30 kHz and sometimes up to 1000 kHz. Therefore, low frequency (LF; 30–300 kHz) and medium frequency (MF; 300–3000 kHz) receivers tend to detect impulsive rather than continuous auroral hiss. The lower cutoff frequency of auroral hiss detected by ground-based instruments is often about 4 kHz [*Helliwell*, 1969] but can be as low as below 1 kHz [*Makita*, 1979, p. 6], or as high as 10 to a few hundred kilohertz [*Morgan*, 1977b; *LaBelle et al*., 1998]. Hiss events with a higher cutoff frequency are called "LF cutoff" by *LaBelle et al*. [1998] and amount to a third of the LF hiss observed at Antarctic stations.

[3] High-resolution ground-based observations show the fine structure of the hiss events in both time and frequency [e.g., *Siren*, 1975; *Ungstrup and Carpenter*, 1974; *Sonwalkar and Harikumar*, 2000; *Ye and LaBelle*, 2008]. The fine structure changes on sub-second time scales. The accepted mechanism for auroral hiss is coherent amplification of whistler mode noise by inverse Landau damping on

[1] Department of Physics and Astronomy, Dartmouth College, Hanover, New Hampshire, USA.
[2] Max-Planck Institut fuer extraterrestrische Physik, Garching, Germany.
[3] Space, Telecommunications, and Radioscience Laboratory, Stanford University, Stanford, California, USA.
[4] Space Science Laboratory, University of California, Berkeley, California, USA.
[5] Department of Physics and Astronomy, Siena College, Loudonville, New York, USA.

Corresponding author: X. Yan, Department of Physics and Astronomy, Dartmouth College, 6127 Wilder Lab, Hanover, NH 03755, USA. (Xi.Yan.gr@dartmouth.edu)

2169-9380/13/10.1002/jgra.50141

the auroral electron beam, which is the source of energy for the emissions [*Maggs*, 1976]. Because it originates in the whistler mode, hiss is generated at altitudes where its frequency is below the local electron gyrofrequency or plasma frequency, whichever is less. This implies sources below 1000 km (f_{pe},f_{ce} $\approx$ 1 MHz) for LF auroral hiss and below about 10,000 km (f_{pe},f_{ce} $\approx$ 30 kHz) for VLF auroral hiss [e.g., Figure 85 of *Makita*, 1979].

[4] Impulsive hiss is related to the onset of auroral substorms [*Makita*, 1979; *LaBelle et al*., 1994] and has primarily been reported on the nightside. It usually coincides with the substorm breakup phase [e.g., *Morozumi*, 1965; *Hayakawa et al*., 1975; *Kokubun et al*., 1972; *Makita*, 1979; *Tanaka et al*., 1976; *Sazhin et al*., 1993; *LaBelle et al*., 1994]. Early observers reported a close correlation between impulsive auroral hiss and occurrences of strong aurorae, enhanced Ap index, perturbations of the geomagnetic field *H* component, etc. [e.g., *Jørgensen and Ungstrup*, 1962; *Jørgensen*, 1964; *Harang and Larsen*, 1965; *Makita*, 1979]. Auroral hiss occurrence rates maximize for moderate Kp index, which reflects the global geomagnetic activity, and decrease at higher or lower Kp [e.g., Figure 8 of *Gurnett*, 1966; *Hayakawa et al*., 1975; *Tanaka et al*., 1976]. Ground-based observations show that the auroral hiss usually happens at night magnetic local time and peaks pre-midnight at both VLF [e.g., *Jørgensen*, 1966; *Harang and Larsen*, 1965; *Hayakawa et al*., 1975; *Kokubun et al*., 1972; *Morgan*, 1977a,b; *Makita*, 1979] and LF [*Morgan*, 1977b; *LaBelle et al*., 1998], although some of these previous observations do show evidence that VLF auroral hiss occurs on the dayside as well [e.g., Figures 1 and 4 of *Jørgensen*, 1966; Figure 3 of *Ondoh*, 1991]. In addition, some individual daytime hiss events have been studied [e.g., *Egeland et al*., 1987; *LaBelle et al*., 1998]. Some data suggest that satellite-based measurements reveal hiss events over a broader range of local times than the ground-based measurements [see Figure 3 and related discussion in *LaBelle and Treumann*, 2002].

[5] The LF auroral hiss events studied in this paper were measured with the Dartmouth College LF/MF/HF receiver at South Pole Station. The sensor is a 10 m^2 magnetic loop placed about 1 km from the station and oriented to minimize local interference. The pre-amplified signal is transmitted by coaxial cable to several data acquisition systems. The one used in this paper, called the Programmable Frequency Receiver (PFR), provides continuous 0–5 MHz spectra with 10 kHz frequency resolution and 2 s time resolution [for more details, see *Weatherwax et al*., 1995]. The geomagnetic latitude of South Pole Station is 74.14°S which puts it in the polar cap just poleward of the auroral zone for some hours around midnight magnetic local time (MLT). Nevertheless, instruments at South Pole register frequent aurora and auroral substorms. The great advantage of South Pole for auroral hiss observations is the minimal manmade interference there, in contrast to Northern Hemisphere observatories which are plagued by interference from LF and AM broadcast signals.

[6] Very low frequency (VLF) hiss is also recorded at South Pole, using an ELF/VLF receiver which records wave activity incident upon two orthogonal magnetic loop antennas. In continuous mode, the system records, twice per second, the average wave amplitude in a set of band-pass-filtered frequency channels from 0.5 to 40 kHz. Broadband data, wherein the receiver output is digitized directly with a sampling frequency f_s = 100 kHz, are recorded synoptically for 1 min out of each 15 starting at 5, 20, 35, and 50 min after the hour. The database of auroral hiss emissions examined below comes from broadband measurements recorded on the East/West antenna, which is less susceptible to manmade noise from the station.

[7] Another significant advantage of South Pole Station is the cluster of ground-based ionospheric instruments located there, including photometers, magnetometers, riometers, and all-sky cameras. The photometer at South Pole has a wide field of view (approximately 55° full angle) centered on the zenith. It includes 630.0 and 427.8 nm interference filters, each with calibrated 3.2 and 2.6 nm passbands, respectively, to observe the corresponding OI 630.0 nm and N_2^+ 427.8 nm emissions. Data are digitally recorded every 1 s during austral winter. Slow variations of the terrestrial magnetic field are measured with a fluxgate magnetometer covering DC to 0.5 Hz, also with a 1 s sampling rate. The magnetometer can measure fluctuations as small as 0.03 nT, although the measured perturbations reported below are of the order of tens of nanotesla, and perturbations associated with magnetic storm effects often exceed 1000 nT. The three axes are oriented in the geomagnetic south-north, west-east, and vertical directions. The South Pole broadbeam riometer operates on 38.2 MHz. The field of view, approximately 60° full angle centered on the zenith, is approximately a circular area of 100 km diameter at 90 km altitude which corresponds to the stopping height of 30 keV precipitated electrons. Finally, the South Pole all-sky imager (ASI) [*Ebihara et al*., 2007] consists of a 180° field-of-view fish-eye lens (f = 6 mm, F = 1.4), an automated filter changer, and a back-illuminated, air-cooled CCD camera with the resolution set at 512 × 512 pixels for the 630.0 and 557.7 nm filters and 256 × 256 pixels for the 427.8 nm filter. For about 4 months of the austral winter, when the Sun lies more than 12° below the horizon, the ASI obtains images on a 51 s cadence during clear-sky conditions.

2. Data Presentation

[8] Figure 1a shows a 25 min, 30–450 kHz spectrogram recorded at South Pole Station during daytime pre-noon MLT. (Midnight MLT corresponds to 03:35 UT.) Spectral peaks at 160–180 kHz and 230–290 kHz are interference, most likely generated in the station. The impulsive events at 12:51-2 UT and 13:06-7 UT, which repeat every 15 min, result from an active beacon experiment. A typical dayside LF hiss event occurs at 12:59 UT (09:24 MLT). It spans from below 30 to above 200 kHz and lasts about 1 min. Additional weaker dayside LF hiss bursts occur near 12:49 UT, 12:50 UT, and 13:05 UT, as well as a very faint trace of an event at 13:02 UT.

[9] This dayside hiss has frequency-time characteristics similar to those of nightside hiss. (For examples of the latter, see Figures 1–3 in *LaBelle et al*., [1998].) It is similarly impulsive, and its power spectral density decreases with increasing frequency. It extends into the VLF range. In general, dayside hiss events recorded at South Pole in 2004–2005 appear indistinguishable from nightside hiss

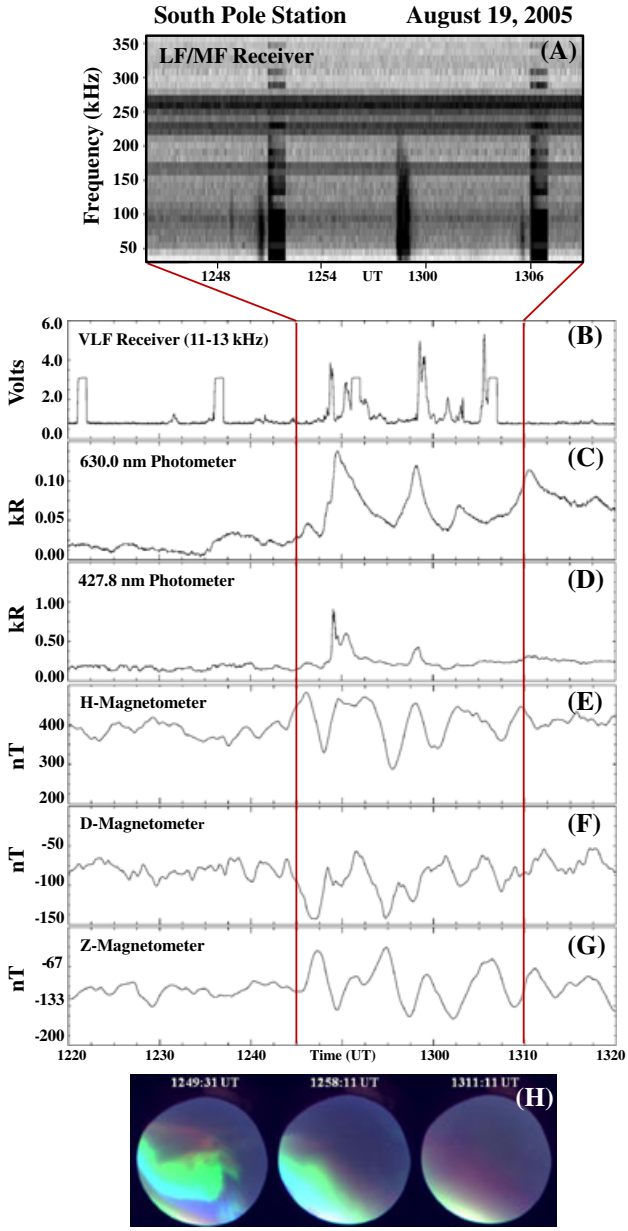

Figure 1. (a) The 0–450 kHz spectrogram of dayside hiss events recorded at South Pole Station during 1245–1310 UT on 19 August 2005; (b–h) corresponding VLF intensity, photometer, magnetometer, and all-sky imager data spanning a wider time interval. In the spectrogram, the gray scale spans 27 dB with white (black) pixels corresponding to 3.2×10^{-15} V^2/m^2 Hz (1.6×10^{-12} V^2/m^2 Hz). In the all-sky images, geographic longitude 0° is to the top and 90° is to the right. The center of the image is at 90°S, i.e., zenith at the South Pole Station.

events in the literature or recorded at South Pole during the same years.

[10] Figures 1b–1h show other relevant geophysical data recorded at South Pole Station at 12:20–13:20 UT, spanning the time of the dayside hiss event. The most reliable correlation is between dayside LF hiss at frequencies above 30 kHz, monitored with the Dartmouth PFR, and VLF hiss detected with the Stanford instrument. Figure 1b shows VLF wave power from the Stanford receiver integrated over 11–13 kHz. As in Figure 1a, this channel registers the impulsive interference at 15 min intervals due to the active beacon experiment. It shows clear evidence of the dayside hiss event at 12:59 UT. Furthermore, weaker peaks of VLF hiss coincide with the three weaker peaks of LF hiss at about 12:49 UT, 12:50 UT, and 13:05 UT, as well as weaker hiss at around 13:02 UT. The other Stanford VLF filter bank channels at 0.5–1 kHz, 1–2 kHz, 2–4 kHz, and 31–38 kHz (not shown) also detect the dayside hiss.

[11] Figures 1c and 1d show intensity in kilorayleighs detected by the 630.0 and 427.8 nm wide field-of-view photometers. Small enhancements in emission of both wavelengths, at the level 0.1–0.6 kR, roughly coincide with some of the bursts of VLF and LF dayside hiss. Figures 1e–1g show the *H*, *D*, and *Z* components of the DC magnetic field measured with the fluxgate magnetometer. The magnetometer data show fluctuations in the order of tens of nanotesla, which are not exactly correlated with the auroral hiss. Riometer data (not shown) show no absorption signatures at the time of the auroral hiss. This contrasts with the case of nightside LF hiss events, which nearly always coincide with prompt absorption registered by riometers and a strong negative bay in the magnetometer *H* component characteristic of substorm onset [see, for example, *LaBelle et al.*, 1994]. Figure 1h displays all-sky images obtained from a camera sensitive to three wavelengths, 427.8 nm, 557.7 nm, and 630.0 nm, at three selected times spanning the VLF/LF dayside hiss event, approximately 12:49 UT, 12:58 UT, and 13:11 UT. The images are a composition of the three wavelengths. They show active auroral arcs near or slightly equatorward of the zenith at the time of the hiss, which are undoubtedly the cause of the enhancements in the photometer signals (Figures 1c and 1d).

[12] In summary, this dayside hiss event observed at the South Pole on 19 August 2005 occurs at both LF and VLF, and coincides with photometer and magnetometer signatures, as well as brightenings of an isolated sharply defined auroral arc which fades away after the event observed with the all-sky camera. There is no distinguishing feature in the wave data of this dayside event relative to commonly observed nightside events. However, nightside events are almost always associated with substorm onsets, which is not the case in this dayside event.

[13] The occasional observations of dayside hiss events such as that shown in Figure 1 motivated a statistical study of dayside LF hiss. We developed a computer algorithm to identify candidate hiss events and followed up with manual inspection of spectrograms to confirm the identifications. The detection algorithm focused on the wave power in ninety-eight 10 kHz wide frequency bands spanning 30–1000 kHz. The algorithm started by taking the maximum wave power at each frequency of 10 successive spectra, reducing the effective time resolution from 2 s to 20 s. Second, the algorithm removed repeated impulsive interference, such as the impulses at 12:51–12:52 UT and 13:06–13:07 UT in Figure 1a which are due to local beacon transmissions. Third, for each 10 kHz wide frequency channel, each 20 s, the algorithm determined a noise level defined as the median wave power at that frequency in a sliding 10 min window. (No averaging was performed.) Simultaneous detection of signals exceeding this noise level

by 2.7–3 dB in eight of nine successive frequency channels constituted a candidate hiss event (six of seven for the year 2007 because of higher noise levels, primarily due to increased locally generated manmade noise from South Pole Station). The algorithm first checked 30–110 kHz, then shifted to 40–120 kHz, and so forth. If no event was found within 30–500 kHz, the algorithm stopped. Otherwise, it continued to test sliding 90 kHz frequency ranges up to 1000 kHz. Events identified less than 30 min apart were counted as one event. There was no selection based on the duration of signals because these events were usually short, but the time resolution of the data used in the survey, after the initial step of taking the maxima of 10 spectra, was 20 s. The algorithm recorded year, day of year, start and end time, duration, maximum and minimum frequencies, and maximum and average intensities for each event.

[14] Due to increases in the level of manmade noise recorded at South Pole Station, primarily from local sources, in many years the noise level at South Pole Station was too high for optimal functioning of the hiss detection algorithm, which worked well only for data with relatively low noise in the tested frequency range (30–1000 kHz). From the decade 2000–2010, we obtained best results for three selected years when the noise level was relatively low: 2004 (day of year 153–366), 2005 (day of year 1–290), and 2007 (day of year 1–271). The automatic hiss detection algorithm identified approximately 1243 events from these years; manual inspection of spectrograms reduced the number of events to 1111 because some of the events identified by the algorithm were deemed due to RF interference.

[15] Figure 2 shows the results of the statistical study of LF hiss recorded at South Pole Station in 2004 (shown in black), 2005 (blue), and 2007 (red). As expected, the vast majority of the events occur in the pre-midnight sector. However, there is a secondary peak, consisting of 71 events, in the pre-noon sector (1000–1530 UT), and an even greater number of events occur in the post-noon sector (1530–2100 UT), which merge into the pre-midnight peak. There is a null at noon MLT (approximately 1530 UT). Statistically, the dayside LF hiss events do not extend to as high frequency as do the events in the pre-midnight sector. Specifically, the occurrence rate of nighttime events having frequencies $\geq$500 kHz implies that 8 of 71 pre-noon events should do so, whereas no $\geq$500 kHz pre-noon events occur. The probability of this occurring by chance is less than 10^{-4}.

[16] Figure 3 summarizes the South Pole VLF hiss database collected during 2001–2008. The hiss database was generated using a modified version of the automatic emission detector algorithm developed by *Golden et al.* [2011] for the Stanford ELF/VLF data from Palmer Station, Antarctica. The algorithm performs a number of data cleaning steps, including hum and sferic removal, and then applies a neural network model to categorize the emission spectra. For the South Pole data, the neural network identifies

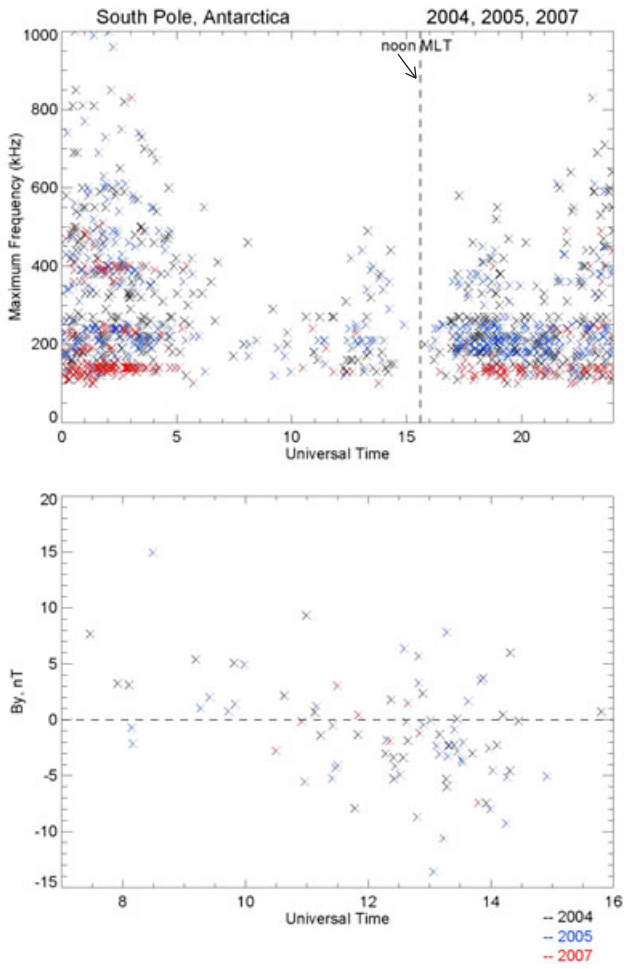

Figure 2. The LF hiss recorded at South Pole Station in 2004 (black crosses), 2005 (blue crosses), and 2007 (red crosses) plotted on a scatter plot of universal time of occurrence (x axis) and maximum frequency (y axis). Noon MLT at South Pole corresponds to 1535 UT. The bottom panel shows a subset of these data, corresponding to 0700–1600 UT, plotted on a scatter plot of IMF B_y component (y axis) versus universal time of occurrence (x axis).

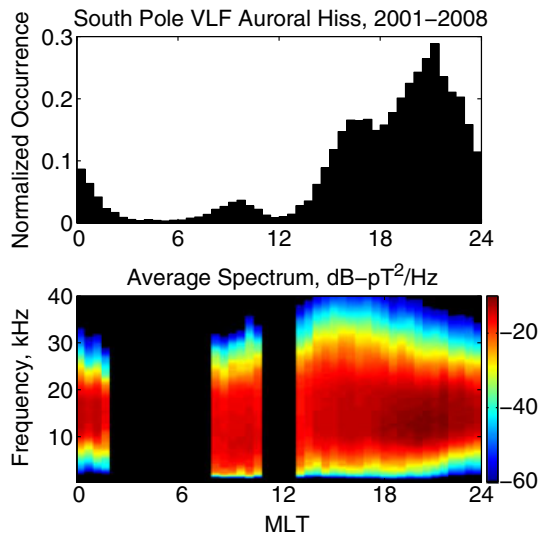

Figure 3. Normalized occurrence of VLF auroral hiss at South Pole, Antarctica from 2001 to 2008 as a function of MLT. The bottom panel shows the average power spectral density of VLF auroral hiss for local times when the normalized hiss occurrence rate exceeds 2%.

chorus and auroral hiss and rejects whistlers and a wide variety of artificial noise. The output of the algorithm is a database of hiss occurrence on a 15 min cadence along with power spectral density of the emission averaged over a 10 s window. For 2001–2008, 188,299 out of 280,320 synoptic records were available for processing, yielding an average data coverage of 67%. The automated algorithm identified 14,018 auroral hiss emissions in that interval. The top panel of Figure 3 shows the normalized hiss occurrence rate as a function of MLT. Similar to the LF hiss results, the occurrence rate maximizes in the pre-midnight sector but shows a small but distinct peak in the pre-noon hours and a larger post-noon peak that merges into the nightside distribution. The bottom panel shows the average power spectral density of VLF auroral hiss for local times when the normalized hiss occurrence rate exceeds 2%, showing that nightside VLF hiss extends to higher frequencies than dayside hiss, as was the case for LF hiss shown in Figure 2.

[17] The 71 pre-noon LF hiss events have been examined in detail. All-sky camera data were available for 31 of these events: 20 events corresponded to overhead auroral arcs, usually isolated, and in 11 of these 20, the aurora was active; three events corresponded to auroral arcs within view but not overhead; two events corresponded to weak aurora; and six events corresponded to indeterminant auroral conditions. One event, on 19 July 2005, was associated with a faint red arc. Photometer data were available for 28 of the 43 events during 2005 and 2007: 21 events coincided with enhancements in at least one photometer channel. Magnetometer, riometer, and VLF signatures were examined for 43 events during 2005 and 2007: 24 of these events were associated with magnetometer signatures, 16 with riometer signatures, and 37 with VLF signatures. A high proportion of the dayside LF hiss events extends to the VLF range, and in some cases VLF signatures occur shortly before or after dayside hiss events which may comprise hiss events observable at VLF only. For 16 selected 2005 events associated with VLF, magnetometer, and photometer signatures, Cluster and ACE satellite data were examined. In one case, 1328 UT on 15 August 2005, a signature resembling a magnetospheric impulse event occurs near the time of the dayside hiss event; in no other cases was there any evidence of solar wind signatures or impulses on the magnetopause at times of these events.

[18] Nightside impulsive LF hiss events are almost always associated with substorm onsets and are concentrated at pre-midnight or midnight hours MLT where substorm activity is most intense. The dayside events are a curiosity in this regard, because they are observed far from the center of the substorm activity. To understand this occurrence pattern better, we performed three statistical studies relating dayside hiss occurrence to IMF conditions. For the first statistical study, we sorted all of the pre-noon LF hiss events and a random sample of the post-noon LF hiss events according to IMF B_y and B_z values determined from ACE satellite data. Two methods were used to calculate the delay time from the satellite to the ionosphere. The first method uses ACE solar wind data propagated according to the methods of *Weimer et al*. [2003]. The delay time from the ACE satellite to the bow shock and the propagated IMF calculated with this method are tabulated at http://vmo.igpp.ucla.edu/data1/Weygand/PropagatedSolarWindGSE/weimer/ACE/TAP. However, this method does not work well when there is a "bad" flag in the ACE data, or when shocks occur. The second method is to calculate the delay time by the measured solar wind speed. The ACE satellite is at the Lagrange point, which is 240 R_E. The bow shock is at 15 R_E, and the magnetopause is at 12 R_E. From the satellite to the bow shock, the time is 225 R_E divided by the solar wind speed. For both methods, an additional delay was included to account for the time from the bow shock to the magnetopause, which is 3 R_E divided by one sixth of the solar wind speed, and yet another 300 s delay was added to account for propagation from the magnetopause to the ionosphere. The results of both methods turned out to be very similar. Table 1 shows the results of the first method. IMF B_y or B_z values "near zero" mean that they lie between about –1 and 1 nT. IMF B_y and B_z values "undetermined" mean that their sign fluctuates on sufficiently short intervals that it cannot be determined given the uncertainty in the time delay calculation. Undetermined IMF B_y and B_z usually happen when they are highly variable. Aside from these cases, Table 1 shows that pre-noon dayside hiss events show a strong (more than 3:1) preference for B_y negative, whereas post-noon events show a strong preference for B_y positive. IMF B_z positive and B_z negative are about equal for pre-noon events, but B_z negative dominates the post-noon events.

[19] The second statistical study is a superposed epoch analysis of IMF B_y and B_z, using LF and VLF hiss events to determine the epoch time. In this study, the IMF parameters with 5 min time resolution are obtained from the *Qin et al*. [2007] solar wind database (http://virbo.org/QinDenton), which is based on satellite data suitably time delayed to account for propagation between the satellite location and the Earth. The epoch time is defined as the midpoint of the start time and end time of each LF hiss event. Figure 4 shows the results for approximately 1100 LF hiss events from 2004, 2005, and 2007. Figures 4a and 4b show IMF B_y and B_z, respectively, as a function of epoch time, sorted into four categories: pre-noon (0630–1200 MLT, red trace), post-noon (1200–1730 MLT, blue trace), nightside (1730–0630 MLT, purple trace), and 500 randomly selected epoch times as a control (black trace). Consistent with the results of Table 1, this analysis reveals a trend in IMF B_y associated with the pre-noon events, which are associated with $B_y < 0$. There is no clear corresponding trend regarding the post-noon events. On the other hand, IMF B_z negative conditions are correlated with both pre-noon and post-noon events, although more strongly with post-noon events.

Table 1. Statistical Study of IMF B_y Component for Pre-noon Hiss Events and a Random Sample of Post-noon Hiss Events

No. of Events	$B_y > 0$	$B_y < 0$	$B_y \approx 0$	B_y Undet.	$B_z > 0$	$B_z < 0$	$B_z \approx 0$	B_z Undet.
Pre-noon events	11	36	5	19	18	20	5	28
Post-noon events	16	7	0	16	2	18	2	17

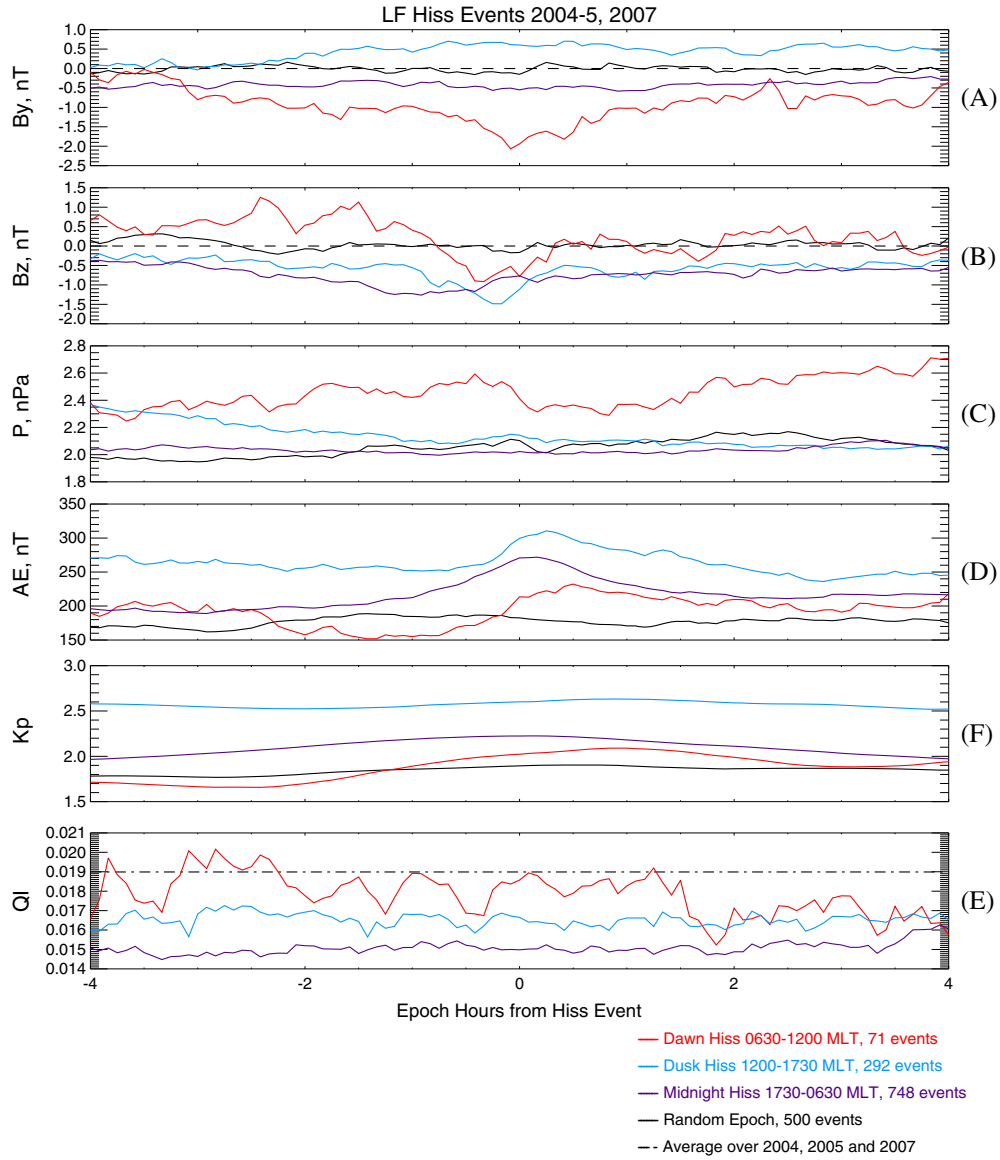

Figure 4. Superposed epoch analyses using LF hiss events as the epoch time: (a) IMF B_y, (b) IMF B_z, (c) solar wind pressure, (d) AE index, (e) Kp index, and (f) QI (see discussion in section 3). Four traces are shown, corresponding to pre-noon LF hiss events (red), post-noon LF hiss events (blue), nightside LF hiss events (purple), and random epoch times (black). The results suggest that pre-noon LF hiss events favor IMF $B_y < 0$; post-noon and pre-noon events favor $B_z < 0$; no clear correlation of either with solar wind pressure; LF hiss at all local times is associated with elevated AE index, although the effect is weak for pre-noon events; and post-noon events are associated with elevated Kp index.

[20] The superposed epoch analysis in Figure 4 suffers from the relatively small numbers of observed LF hiss events. Figure 5 shows a similar superposed epoch analysis based on randomly selected subsets of the far more numerous VLF hiss events. As in Figure 4, the analysis uses the *Qin et al.* [2007] database for IMF parameters and solar wind pressure and divides the hiss events into three local time categories, pre-noon, post-noon, and nightside. The results are similar to those obtained for the LF hiss events, but significantly clearer since in the VLF case 650 events are used in each analysis. Figure 5a suggests that IMF $B_y < 0$ is associated with the pre-noon events and $B_y > 0$ with the post-noon events, in agreement with Figure 4 and Table 1. Figure 5b suggests that both pre-noon and post-noon events are associated with $B_z < 0$, in agreement with Figure 4 and with Table 1 for post-noon events.

[21] As a third statistical study, to quantitatively evaluate the relationships between pre-noon and post-noon auroral hiss events and the sign of IMF B_y and B_z suggested by Table 1, we apply the Mann-Whitney U test [*Mann and Whitney*, 1947] to the database of 1111 LF hiss events used for the superposed epoch analysis in Figure 4. As in the superposed epoch analysis, IMF parameters and solar wind pressure with 5 min cadence are obtained from the *Qin et al.* [2007] solar wind database, and the event times are defined as the midpoint between the start and end

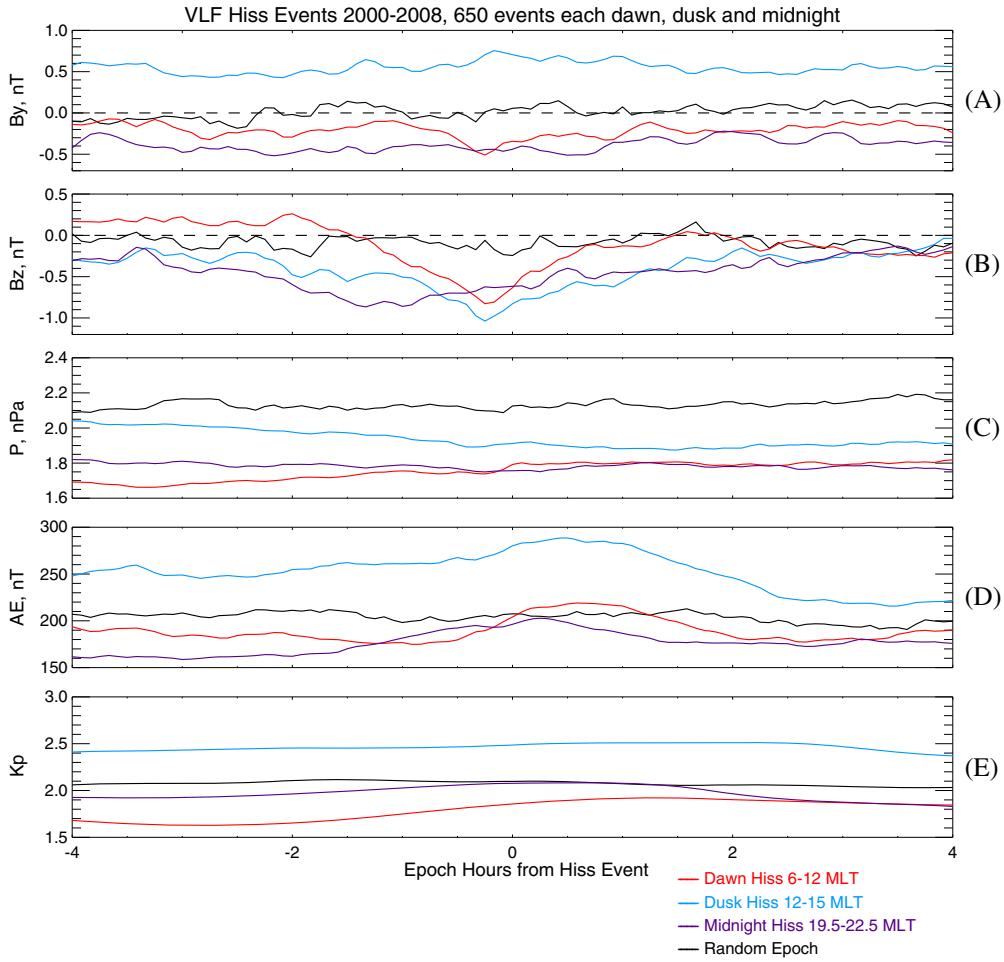

Figure 5. Superposed epoch analyses using VLF hiss events as the epoch time: (a) IMF B_y, (b) IMF B_z, (c) solar wind pressure, (d) AE index, and (e) Kp index. Four traces are shown, corresponding to pre-noon VLF hiss events (red), post-noon VLF hiss events (blue), nightside VLF hiss events (purple), and random epoch times (black). The results suggest that pre-noon VLF hiss events favor IMF $B_y < 0$; post-noon and pre-noon events favor $B_z < 0$; no clear correlation of either with solar wind pressure; post-noon VLF hiss is associated with elevated AE index, with only very weak correlation for other local times; and post-noon events are associated with elevated Kp index.

time of each LF hiss event. We tested five possible dependent variables: IMF B_y, IMF B_z, solar wind pressure, AE index, and Kp index. We ranked pre-noon/post-noon, pre-noon/midnight, and pre-noon/random events according to the values of each dependent variable, calculated U values by the standard method, and used a standard software to interpret the results (at http://elegans.som.vcu.edu/~leon/stats/utest.html) which consist of probability confidence levels (P): $P < 0.05$ implies the two tested data sets differ on the basis of the dependent variable at the 95% confidence level. The results, shown in Table 2, support the conclusions suggested by Table 1 and Figures 4 and 5 that the difference between IMF B_y values for pre-noon and post-noon hiss events is highly significant, with pre-noon hiss events associated with IMF $B_y < 0$ conditions and post-noon events with $B_y > 0$. Similarly, IMF B_y values for pre-noon differ significantly from those for pre-midnight hiss events and random events. On the other hand, there is no significant difference between any of these categories for IMF B_z conditions or for solar wind pressure. The Mann-Whitney test applied to B_z may not be reliable because so many B_z are undetermined.

[22] The IMF B_z statistics in Table 1 and Figures 4 and 5 suggest that post-noon hiss events may be related to substorms. To test the possible role of substorms in the dayside hiss events, substorm conditions at the times of selected events were determined from inspection of IMAGE satellite wideband imaging camera (WIC) pictures of the southern auroral oval. As with the IMF conditions study, data were examined for every pre-noon event and a random selection of post-noon events. The criteria used in the manual inspection were (1) a significant increase in the width of the nightside oval within a few images (10–15 min) of the dayside hiss event, (2) a significant brightening of the nightside aurora within the same time frame, and (3) a significantly increasing or large AE index. Both criteria 1 and 2 had to be present to label the event as coincident with a "substorm," and criterion 3 was most objective and used to check the

Table 2. Results (P Values) of the Mann-Whitney U Test Applied to Combinations of Pre-noon Hiss, Post-noon Hiss, Pre-midnight Hiss, and Random Events Ranked as a Function of IMF-B_y, IMF-B_z, Solar Wind Pressure, AE Index, and Kp Index[a]

	IMF B_y	IMF B_z	SW Pressure	AE Index	Kp Index
Pre-noon versus post-noon	$P < 0.001$	$P \geq 0.05$	$P \geq 0.05$	$P < 0.001$	$P < 0.001$
Pre-noon versus nightside	$P < 0.01$	$P \geq 0.05$	$P < 0.05$	$P \geq 0.05$	$P < 0.05$
Pre-noon versus random	$P < 0.001$	$P \geq 0.05$	$P < 0.05$	$P < 0.001$	$P \geq 0.05$

[a] $P < 0.05$ implies the two data sets differ on the basis of the dependent variable at the 95% confidence level.

Table 3. Statistical Study of Presence of Substorm-like Conditions, as Observed in IMAGE WIC Data, During Pre-Noon Hiss Events and a Random Selection of Post-noon Hiss Events

No. of Events	Non-Substorm	Substorm	Recovery Phase
Pre-noon events	19	9	1
Post-noon events	8	11	3

result from criteria 1 and 2. These criteria of course do not guarantee that a substorm is in progress but are indicative of intense activity in the midnight sector resembling a substorm. Two authors (XY and JL) independently examined the WIC data, and 27 uncertain cases were referred to a third author (HF). Table 3 summarizes the results of this study. More than 50% of the post-noon events coincide with either an ongoing substorm or the aftermath of a substorm, suggesting that a significant portion of the post-noon hiss events may be correlated with substorms, as is also suggested by the way that the local time distribution of the post-noon events merges into the pre-midnight peak in occurrence of nightside events, which are known to be associated with substorms. For the pre-noon events, non-substorm conditions outnumber substorm-like conditions by about two to one.

[23] Another indicator of geomagnetic activity including substorm activity is the Kp index. Figure 6 shows the average of the Kp index for 3 h intervals corresponding to each of more than 1000 hiss events shown in Figure 1, binned according to universal time. (Noon MLT corresponds to 1530 UT.) The error bars show one standard deviation from the mean. There is only one event during 15–16 UT, so no error bar is shown in this interval. Compared to the pre-noon events, the post-noon and midnight events correspond to elevated Kp values. In the case of nightside events, this is not surprising since they are known to be associated with substorms and have long been associated with elevated Kp [e.g., *Makita*, 1979]. The higher Kp values corresponding to post-noon versus pre-noon events support the data of Tables 1 and 3 showing that the post-noon events, unlike the pre-noon ones, tend to coincide with activity on the nightside and IMF B_z negative conditions.

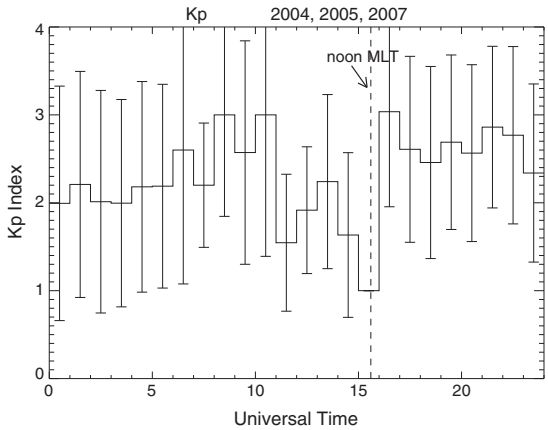

Figure 6. Averages of 3 h Kp indices associated with LF auroral hiss events observed at South Pole in 2004, 2005, and 2007, binned according to universal time. (Noon MLT corresponds to 1530 MLT.)

[24] The other statistical studies support the relationship between post-noon hiss events and substorms suggested by Figure 6 and Table 3. The superposed epoch analyses (Figures 4 and 5) suggest that post-noon hiss events are associated with elevated Kp index, whereas pre-noon events are not. A similar result holds with regard to AE index. In both cases, the effect is expressed better in the VLF superposed epoch analysis (Figure 5) which uses far more events. The superposed epoch analyses both also support the correlation of post-noon events with IMF $B_z < 0$; interestingly, they suggest a correlation in the case of pre-noon events as well, although the effect is weaker. When ranking by AE and Kp indices, there are significant differences between pre-noon and post-noon or pre-midnight events, supporting the suggestion that post-noon and pre-midnight events favor times of strong activity monitored by these indices, whereas pre-noon events do not.

3. Discussion

[25] In the statistical study of LF hiss based on 2004, 2005, and 2007 South Pole data, 71 pre-noon (10:00–15:30 UT) hiss events and 292 post-noon (15:30–21:00 UT) events were found in 775 days. Hence, pre-noon hiss events are relatively uncommon (0.092 events per day on average) compared to post-noon events (0.38 events per day). There is a significant gap in occurrence of dayside hiss at noon MLT: only two hiss events occur in the interval 14:28–16:07 UT, while comparable length intervals immediately before and after the gap have 40 hiss events (12:48–14:28 UT) and 58 hiss events (16:07–17:47 UT), respectively. The statistical study of VLF hiss over a longer time interval (2000–2008) gives similar results (Figure 3 above), with slightly lower occurrence rates but a similar ratio of occurrence for pre-noon versus post-noon events. Previous determinations of the diurnal dependence of VLF hiss occurrence rates are consistent with these features, although they do not resolve them as clearly [see, for example, Figures 1 and 4 of *Jørgensen*, 1966]. Interestingly, a "mid-day gap"

in discrete aurora around noon MLT has also been reported [*Dandekar and Pike*, 1978]. According to *Newell et al*. [2005], this mid-day gap is shifted slightly (about half hour) toward the morning MLT sector. The LF hiss diurnal dependence (Figure 2) also shows evidence that the mid-day null is shifted slightly to pre-noon.

[26] In addition to MLT distributions shown in Figures 2 and 3 above, day-of-year distributions of LF auroral hiss have been investigated. The only significant features of those distributions are decreased event occurrence rates during the first few months of 2007 and the last few months of 2004, times of sunlight at South Pole; 2005, however, showed no such decreased occurrence rates. These effects imply that, were event occurrence rates to be recalculated excluding sunlit time intervals, the occurrence rates of morning-sector LF hiss would be slightly higher; excluding sunlit days from the superposed epoch analysis yields no significant differences from the results shown in Figure 4.

[27] Dayside LF hiss events show a significant correlation with IMF B_y. Pre-noon events favor $B_y < 0$, while post-noon events favor $B_y > 0$. Superposed epoch analysis of both LF and VLF data (Figures 4 and 5) provides further evidence of this correlation.

[28] Two mechanisms could explain this correlation. First, polar cap flows have a well-known dependence on IMF B_y [e.g., *Haaland et al*., 2007]. Figure 7, reprinted from Figure 1 of *Gosling et al*. [1990], shows geometries of field line merging in GSM coordinates. The reconnection of closed and IMF field lines produces north lobe and south lobe field lines. For B_y negative cases, the south lobe is pulled azimuthally along the auroral oval in the pre-noon sector, a condition that maximizes energy dissipation, including, presumably, auroral hiss. Similar conditions prevail in the post-noon sector for B_y positive. Near-noon, reconnected field lines would be pulled directly across the polar cap and not be dragged along the auroral oval. The asymmetry of polar cap flow with regard to IMF B_y appears clearly in statistical maps produced with Cluster EDI electric field data [Figure 8 of *Haaland et al*., 2007]. Consistent with the sketch in Figure 7, there is an inverse asymmetry in the northern polar cap flow with a shift toward the pre-noon sector for positive IMF B_y [Figure 7 of *Haaland et al*., 2007].

[29] An alternative explanation involves the latitude and local time dependence of auroral field aligned currents (FACs). *Wing et al*. [2010] present statistical locations of upward and downward FACs based on DMSP magnetic field measurements in the Northern Hemisphere. Their Figure 6 shows that for $B_y > 0$ the pre-noon pattern belonging to the auroral oval is shifted toward the afternoon sector in the Northern Hemisphere. This is opposite to the behavior of the polar cap flow discussed above and shown in Figure 7. Assuming that the same inverse asymmetry holds as for the polar cap flow, we conclude that the auroral FACs are shifted from pre-noon toward afternoon on the Southern Hemisphere for $B_y < 0$. Strong support for the inverse behavior of oval and polar cap flows under B_y dependence can be found in Figure 10b of *Cowley and Lockwood* [1992]. Specifically, Figure 6 of *Wing et al*. [2010] shows that for 74° invariant latitude, corresponding to South Pole Station, Region 2 (upward) FACs are much more prominent in the pre-noon hours for $B_y > 0$ than for $B_y < 0$ in the Northern Hemisphere. Thus in the Southern Hemisphere, the upward FACs will dominate the pre-noon hours for $B_y < 0$ at 74° invariant. This supports the observed correlation between IMF and dayside auroral hiss, i.e., the preference for $B_y < 0$ in the pre-noon hours. But this explanation is linked to the upward FACs of the auroral oval rather than to the polar cap flow.

[30] To distinguish these hypotheses requires using local magnetometer data to determine where the South Pole Station lies with respect to auroral currents during the dayside hiss events. The forenoon region should be dominated by westward horizontal currents and southward electric fields since the downward FACs are located further poleward. From 24 h summary plots, the baseline of the H component of the local magnetic field was determined, which then allowed classification of events according to whether the H component lies >10–20 nT above or below the baseline. A survey of approximately 30 randomly selected pre-noon events reveals that about 50% correspond to negative ΔH (H component below baseline), i.e., westward Hall currents, and 50% to $\Delta H \approx 0$ (at baseline to within 10–20 nT). At most one event, counted as a zero, is borderline positive (above baseline). In contrast, a similar survey of post-noon events showed a rather different distribution; these are predominantly at baseline (about 75%), with most of the rest corresponding to negative ΔH (below baseline), with one or two (out of 35 in the sample) possibly borderline positive ΔH (above baseline). These data support the role of auroral currents, rather than polar cap flows, determining

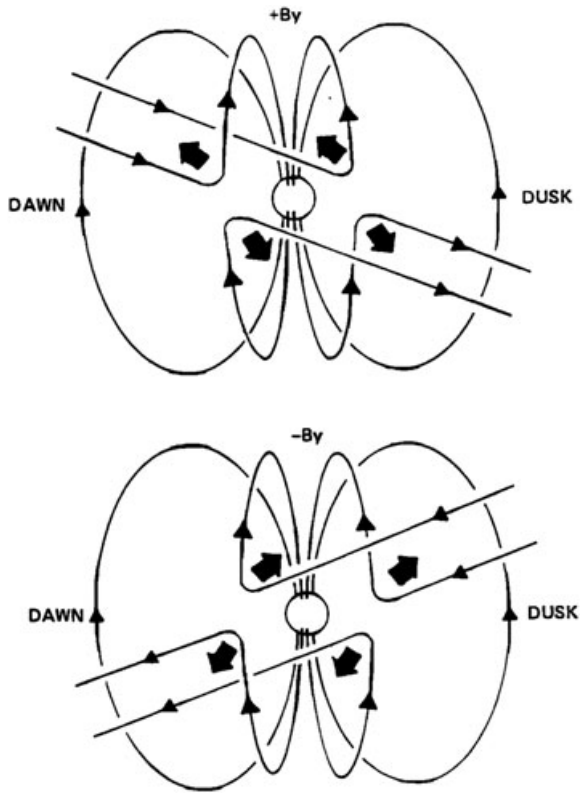

Figure 7. The reconnection configurations for different IMF-B_y conditions, reprinted from Figure 1 of *Gosling et al*. [1990].

the dayside hiss IMF B_y dependence, although in the case of post-noon events, associated with high Kp index, it is possible that they correspond to the narrow band of eastward convection at the polar boundary of the auroral oval [see *Fujii et al*., 1994].

[31] The IMF $B_y < 0$ therefore shifts the region of upward field-aligned current closer to mid-day, leading to more hiss events with $B_y < 0$ in the immediate pre-noon hours. At still earlier local times, however, including most of the time after about midnight or 02 MLT, the station at 74° is in the downward current region of the R1 system for IMF $B_y < 0$, implying that the IMF control should show an MLT dependence. Figure 2 (bottom panel), an expanded plot of IMF B_y versus MLT for the pre-noon dayside hiss events, shows that this prediction is indeed borne out by the data: The tendency to favor the condition $B_y < 0$ occurs primarily near noon.

[32] A good indicator of sunspot-cycle information contained in the solar wind is the solar wind Quasi Invariant (QI). QI = $(B^2/8\pi)/(\rho v^2/2) = {M_A}^{-2}$ (1) where B, ρ, and v are the magnetic field, plasma density, and bulk speed of the solar wind. M_A is the magnetic Mach number. QI is 10–100 times higher for magnetic clouds than for normal solar wind conditions, and also increases during other geo-effective solar wind structures [*Osherovich et al*., 1999; 2007]. Figure 4f shows the results of a superposed epoch analysis of QI, using LF auroral hiss events as the fiducial. The horizontal dashed line in Figure 4f shows the average QI over the applicable time interval. Because of the variability of QI over the solar cycle, there is a great deal of variation in the analysis of the dawn and dusk hiss events that results from the small sample size and may not be real. The only possibly significant feature of the analysis is the distinctly diminished QI values associated with the midnight LF hiss events, for which there are more samples and for which the superposed epoch analysis shows much less variation. The most likely explanation for this feature is that the relatively high magnetic latitude of South Pole Station (74° invariant) at midnight lies poleward of the auroral oval and associated upward field-aligned currents under most conditions. *Mende et al*. [1999] analyze substorm activity at South Pole and comparably high latitude observatories, finding that about 20% of substorms occurring in the appropriate geographic sector penetrate above 80° invariant latitude during 1994–1995 (near solar minimum), although there were fewer such poleward penetrations near midnight. Interestingly, there was no evidence for a strong influence of IMF-B_z on the occurrence of high-latitude substorms. *Mende et al*. [1999] suggest competing effects: the passage of a magnetic cloud or other geo-effective event is often associated with buildup of magnetic storms and substantial widening of the polar cap, with the region of upward FAC moving further equatorward of 74°, but "under these conditions we also expect larger poleward auroral expansions which can reach high latitudes." The overall effect of IMF-B_z (or QI) could therefore go either way; Figure 4f suggests that in the case of QI, the southward shift of the oval during geo-effective events may be the more significant effect leading to decreased auroral hiss at 74° invariant in the midnight sector.

[33] Several lines of evidence suggest that pre-noon dayside hiss events may be distinct from post-noon events. The post-noon events correspond to elevated average Kp values relative to the pre-noon events (Figure 6), and the average Kp values for the post-noon events are in fact comparable to those for nighttime auroral hiss events which are known to occur at substorm onsets. Examination of IMAGE WIC images of the auroral oval during pre-noon and post-noon events shows a tendency for the latter to more often coincide with substorm-like activity in the nightside oval. Taken together, these data suggest that a large portion of the post-noon hiss events may be associated with substorm expansions on the nightside, whereas the pre-noon events are mostly independent of substorm activity. This conclusion is also suggested by the way that the local time distribution of the post-noon events merges into the pre-midnight peak in occurrence of nightside events, which are known to be associated with substorms.

[34] In summary, Figure 2 and the IMF B_y dependence of dayside auroral hiss can be explained as follows: (1) auroral hiss is connected to upward FAC of the auroral oval; (2) South Pole Station at 74° is in the upward FAC region of the Region 1 (R1) currents between early afternoon and shortly after midnight, and otherwise predominantly in the downward section of the R1 system; (3) during pre-noon MLT, the station sometimes finds itself under the upward FACs of the Region 2 system, more so for IMF $B_y < 0$; and (4) during a few hours around noon, the station is in the so-called throat flow from dayside into the polar cap with little energetic electron precipitation. Finally, this study of dayside auroral hiss also suggests that nightside substorm activity and IMF B_z influence post-noon dayside hiss events more than pre-noon events.

[35] The superposed epoch analysis (Figures 4 and 5) indicates that AE index peaks 0.5–1 h after the epoch time, B_z negative maximizes approximately 0.25 h before the epoch time, and Kp index peaks approximately 1 h after the epoch time for pre-noon events only. It is not surprising that B_z negative maximizes shortly before the hiss activity, since the magnetosphere requires some period of solar wind driving prior to substorm onset. More significantly, B_z begins to turn negative about 45 min prior to the epoch time, a correlation that may result because LF hiss occurs not during the growth phase, which typically has a duration of this order, but after substorm onset. The peak in AE less than half hour after epoch time for midnight and evening hiss suggests that those hiss events occur during substorm expansion phase; the peak in AE in the case of pre-noon (dawn) hiss is interesting that it exists at all, because it suggests a connection to substorm activity, and its delayed timing suggests that dawn hiss occurs preferentially close to substorm breakup.

[36] Incidentally, the LF hiss statistics in Figure 2 suggest a dependence of the maximum hiss frequency on the year, with 2004–2005 generally corresponding to higher maximum frequencies than 2007. The percentages of the hiss events with a maximum frequency within 600–1000 kHz are 0.0503 (19 out of 378 events) for 2004, 0.0503 (23 out of 457 events) for 2005, and 0.0036 (1 out of 276 events) for 2007. This trend indicates that auroral hiss sources cover a wider range of altitudes, in particular extending deeper into the ionosphere, in the declining years of the solar cycle (2004–2005) compared to the depth of solar minimum (2007).

[37] **Acknowledgments.** Work at Dartmouth College was supported by NSF Office of Polar Programs awards ANT-1043230 and ANT-1141817. Work at Stanford University was supported by NSF Office of Polar Programs awards ANT-0840058, ANT-1043442, and ANT-1141791. Work at Siena College was supported by NSF Office of Polar Programs awards ANT-0638587 and ANT-0840158. GH is grateful to the Harris Foundation for the opportunity to visit Dartmouth College in Fall 2011.

References

Burton, E. T., and E. M. Boardman (1933), Audio-frequency atmospherics, *Proc. Inst. Radio Eng.*, *21*, 1476.

Cowley, S. W. H., and M. Lockwood (1992), Excitation and decay of solar wind-driven flows in the magnetosphere-ionosphere system, *Ann. Geophys.*, *10*, 103–115.

Dandekar, B. S., and C. P. Pike (1978), The midday, discrete auroral gap, *J. Geophys. Res.*, *83*, 4227–4236, doi:10.1029/JA083iA09p04227.

Ebihara, Y., Y.-M. Tanaka, S. Takasaki, A. T. Weatherwax, and M. Taguchi (2007), Quasi-stationary auroral patches observed at the South Pole Station, *J. Geophys. Res.*, *112*, A01201, doi:10.1029/2006JA012087.

Egeland, A., H. Liao, and P. E. Sandholt (1987), Irregular, broad-band ELF/VLF emissions and optical aurora at cusp latitudes in the post-noon sector, *Annales Geophys.*, *5*, 89.

Fujii, R., R. A. Hoffman, P. C. Anderson, J. D. Craven, Sugiura, M., L. A. Frank, and N. C. Maynard (1994), Electrodynamic parameters in the nighttime sector during auroral substorms, *J. Geophys. Res.*, *99*, 6093. exit

Gallet, R. M. (1959), The VLF emissions generated in the Earth's exosphere, *Proc. Inst. Radio Eng.*, *47*, 211.

Golden, D. I., M. Spasojevic, and U. S. Inan (2011), Determination of solar cycle variations of mid-latitude ELF/VLF chorus and hiss via automated signal detection, *J. Geophys. Res.*, *116*, A03225, doi: 10.1029/2010JA016193.

Gosling, J. T., M. F. Thomsen, S. J. Bame, R. C. Elphic, and C. T. Russell (1990), Plasma flow reversals at the dayside magnetopause and the origin of asymmetric polar cap convection, *J. Geophys. Res.*, *95*(A6), 80738084, doi:10.1029/JA095iA06p08073.

Gurnett, D. A. (1966), A satellite study of VLF hiss, *J. Geophys. Res.*, *71*, 5599.

Haaland, S. E., G. Paschmann, M. Forster, J. M. Quinn, Torbert, R. B., C. E. McIlwain, H. Vaith, P. A. Puhl-Quinn, and C. A. Kletzing (2007), High-latitude plasma convection from Cluster EDI measurements: Method and IMF-dependence, *Ann. Geophys.*, *25*, 239–253, doi: 10.5194/angeo-25-239-2007.

Harang, L., and R. Larsen (1965), Radio wave emissions in the V.L.F.-band observed near the auroral zone: 1. Occurrence of emissions during disturbances, *J. Atmos. Terr. Phys.*, *27*, 481.

Hayakawa, M., Y. Tanaka, and J. Ohtsu (1975), The morphologies of low-latitude and auroral VLF hiss, *J. Atmos. Terr. Phys.*, *37*, 517.

Helliwell, R. A. (1969), Low-frequency waves in the magnetosphere, *Rev. Geophys.*, *7*, 281.

Jørgensen, T. S., and E. Ungstrup (1962), Direct observation of correlation between aurorae and hiss in Greenland, *Nature*, *194*, 462.

Jørgensen, T. S. (1964), Some observations of VLF-hiss and correlated phenomena, *J. Atmos. Terr. Phys.*, *26*, 626.

Jørgensen, T. S. (1966), Morphology of VLF hiss zones and their correlation with particle precipitation events, *J. Geophys. Res.*, *71*, 1367.

Kokubun, S., K. Makita, and T. Hirasawa (1972), VLF-LF hiss during polar substorm, *Geophys. Res. Lett.*, *26*, 138.

LaBelle, J., and R. A. Treumann (2002), Auroral radio emissions, 1. Hisses, roars, and bursts, *Space Sci. Rev.*, *101*, 295–440.

LaBelle, J., A. T. Weatherwax, J. Perring, E. Walsh, Trimpi, M. L., and U. S. Inan (1998), Low-frequency impulsive auroral hiss observations at high geomagnetic latitudes, *J. Geophys. Res.*, *103*, 20459.

LaBelle, J., A. T. Weatherwax, M. L. Trimpi, R. Brittain, R. D. Hunsucker, and J. V. Olson (1994), The spectrum of LF/MF/HF radio noise at ground level during substorms, *Geophys. Res. Lett.*, *21*, 2749.

Maggs, J. E. (1976), Coherent generation of VLF hiss, *J. Geophys. Res.*, *81*, 1707.

Makita, K. (1979), VLF/LF hiss emissions associated with aurora, *Mem. Nat. Int. Polar Res.*, *16*, 1.

Mann, H. B., and D. R. Whitney (1947), On a test of whether one of two random variables is stochastically larger than the other, *Ann. Math. Statist.*, *18*, 50.

Martin, L. H., R. A. Helliwell, and K. E. Marks (1960), Association between aurorae and VLF hiss observed at Byrd Station, Antarctica, *Nature*, *187*, 751.

Mende, S. B., H. U. Frey, S. P. Geller, and J. H. Doolittle (1999), Multistation observations of auroras: Polar cap substorms, *J. Geophys. Res.*, *104*, 2333–2342, doi:10.1029/1998JA900084.

Morgan, M. G. (1977a), Auroral hiss on the ground at L = 4, *J. Geophys. Res.*, *82*, 2387.

Morgan, M. G. (1977b), Wide-band observations of LF hiss at Frobisher Bay (L = 14.6), *J. Geophys. Res.*, *82*, 2377.

Morozumi, H. M. (1965), Diurnal variations of auroral zone geophysical disturbances, *Rep. Ionosph. Space Res., Japan*, *19*, 286.

Newell, P. T., S. Wing, and C.-I. Meng (2005), Spectral properties and source regions of dayside electron acceleration events, *J. Geophys. Res.*, *110*, A11205, doi:10.1029/2005JA011264.

Ondoh, T. (1991), Polar hiss observed by ISIS satellites, in *Magnetospheric Substorms*, edited by Kan, J. et al., Geophysical Monograph 64, American Geophysical Union, Washington, DC, p. 387.

Osherovich, V. A., J. Fainberg, and R. G. Stone (1999), Solar wind quasi-invariant as a new index of solar activity, *Geophys. Res. Lett.*, *26*, 2597–2600, doi:10.1029/1999GL900583.

Osherovich, V. A., R. F. Benson, J. Fainberg, J. L. Green, Garcia, L., S. Boardsen, N. Tsyganenko, and B. W. Reinisch (2007), Enhanced high-altitude polar cap plasma and magnetic field values in response to the interplanetary magnetic cloud that caused the great storm of 31 March 2001: A case study for a new magnetospheric index, *J. Geophys. Res.*, *112*, A06247, doi:10.1029/2006JA012105.

Qin, Z., R. E. Denton, N. A. Tsyganenko, and S. Wolf (2007), Solar wind parameters for magnetospheric magnetic field modeling, *Space Weather*, *5*, S11003, doi:10.1029/2006SW000296.

Sazhin, S. S., K. Bullough, and M. Hayakawa (1993), Auroral hiss: A review, *Planet. Space Sci.*, *41*, 153.

Siren, J. C. (1975), Fast hisslers in substorms, *J. Geophys. Res.*, *80*, 93.

Sonwalkar, V. S., and J. Harikumar (2000), An explanation of ground observations of auroral hiss: Role of density depletions and meter scale irregularities, *J. Geophys. Res.*, *105*, 18867

Tanaka, Y., M. Hayakawa, and M. Nishino (1976), Study of auroral VLF hiss observed at Syowa Station, Antarctica, *Mem. Nat. Int. Polar Res.*, *13*, 1.

Ungstrup, I. M., and D. L. Carpenter (1974), Hisslers: Quasi-periodic (t = 2 s) VLF noise forms at auroral latitudes, *J. Geophys. Res.*, *79*, 5196.

Weatherwax, A. T., J. LaBelle, M. L. Trimpi, R. A. Treumann, J. Minow, and C. Deehr (1995), Statistical and case studies of radio emissions observed near 2fce and 3fce in the auroral zone, *J. Geophys. Res.*, *100*, 7745.

Weimer, D. R., D. M. Ober, N. C. Maynard, M. R. Collier, D. J. McComas, N. F. Ness, C. W. Smith, and J. Watermann (2003), Predicting interplanetary magnetic field (IMF) propagation delay times using the minimum variance technique, *J. Geophys. Res.*, *108*, 1026, doi: 10.1029/2002JA009405.

Wing, S., S. Ohtani, P. T. Newell, T. Higuchi, G. Ueno, and J. M. Weygand (2010), Dayside field-aligned current source regions, *J. Geophys. Res.*, *115*, A12215, doi:10.1029/2010JA015837.

Ye, S., and J. LaBelle (2008), Ground-based observations of low frequency auroral hiss fine structure, *J. Geophys. Res.*, *113*, A01313, doi: 10.1029/2007JA012473.